

GT2011-46' ' \$

MODELING OF THE HEAT FLUX FOR MULTI-HOLE COOLING APPLICATIONS

Guillaume Cottin*

Turbomeca
seconded to ONERA/DMAE
Email: guillaume.cottin@onera.fr

Emmanuel Laroche

ONERA/DMAE
2, avenue Edouard-Belin
31055 Toulouse, France
Email: Emmanuel.laroche@onera.fr

Nicolas Savary

Turbomeca
avenue Joseph-Szydowski
64511 Bordes, France
Email: nicolas.savary@turbomeca.fr

Pierre Millan

ONERA/DMAE
2, avenue Edouard-Belin
31055 Toulouse, France

ABSTRACT

The aims of this work are to achieve a better understanding of thermal fluxes around a multi-perforated plate and obtain correlations for heat transfer coefficient on the hot as well as cold side and in a perforation. A 3-dimensional, RANS, conjugate simulation and an adiabatic one are performed for different aerothermal conditions already studied experimentally. Convective heat flux, wall temperature and adiabatic temperature are averaged on a periodic pattern around each hole. A mean heat transfer coefficient is calculated based on these quantities and correlations are deduced for this coefficient. Such results as fluid temperature rise in a perforation or the contribution of flux in the perforations to the whole cooling flux are also given in this article.

NOMENCLATURE

C_p Specific heat capacity
 d Hole diameter
 h Heat transfer coefficient
 H Enthalpy
 l Hole length

Nu Nusselt number
 p Lateral distance between two holes
 Pr Prandtl number
 Re Reynolds number
 s Streamwise distance between two holes
 St Stanton number
 T Temperature
 U_c Streamwise velocity at the centre of cold channel
 U_h Streamwise velocity at the centre of hot channel
 U_j Mean velocity in the perforation
 U_x, U_y, U_z Velocity components
 x, y, z Cartesian coordinates
 y^+ dimensionless wall distance
 α Hole surface angle
 ΔP Pressure difference between hot and cold side
 λ Thermal conductivity
 μ Dynamic viscosity
 Φ Heat flux
 ρ Density
Subscript
 ad Adiabatic
 c Cold flow
 d Parameter calculated from the hole diameter

*Address all correspondence to this author.

h Hot flow
j Jet
w Wall

1 INTRODUCTION

The last 30 years have seen an improvement of the performance of gas turbine. This means an increase of temperature and pressure in the combustion chamber whose liners are submitted to large thermal constraints. Moreover, since 1999, emissions of NOx have to be reduced, this can be achieved with a lean-burn combustion but less air is available for cooling.

To increase the lifetime of the chamber, a cooling method has to be used. Transpiration cooling has been proved to be the most efficient one [1], but porous walls, due to their mechanical weakness, can not be used in gas turbine. An alternative, currently used to protect the liner of the combustion chamber, is the so-called full coverage film cooling (FCFC). It consists of introducing "cold" air from the casing into the chamber through thousands of sub-millimeter angled perforations. The resulting jets coalesce and create a film that protects the internal face from burnt gases.

To optimize the efficiency of this cooling method, computational fluid dynamics is widely used by combustion chamber manufacturers. Nevertheless, the number of perforations is far too large and makes the calculation very expensive. But due to their important effects on the flow, especially by changing the location of the flame, they have to be taken into account.

An appropriate wall model is needed to reproduce the effects of the multi-perforated wall. It will replace the perforated plate by an homogeneous boundary condition. Such a model has already been done by Mendez [2] for the aerodynamic effects, the aim of our work is to study and model the heat fluxes around the plate. To do so, RANS computations have been performed to build a database of five aerothermal conditions. The results have been post processed to learn more about heat fluxes at the wall and obtain correlations for the heat transfer coefficient on the different sides of the plate.

2 PREVIOUS WORK

2.1 Experimental studies

Heat transfer over a perforated plate have been experimentally studied over the past decades. The cold side was studied by Sparrow [3] and Dorignac [4] with cold air injected from a plenum. They give a correlation for the Nusselt number on a reference surface around the hole. But in these experiments, there is no flow in the streamwise direction, which is not representative of full coverage film cooling. Byerley [5] showed the effects of suction ratio on the heat transfer coefficient. Only one hole is considered but it brings to light a region of enhancement of the heat transfer coefficient downstream of the hole. Enhancement

depends strongly of the suction ratio and can be explained by an increase of the velocity and temperature gradient due to suction of the boundary layer through the hole. Heat transfer in perforations had been looked at by Cho [6] who studied the influence of Reynolds number and Dorignac [7] who proposed a correlation for Nusselt number in the hole depending on Reynolds number and the position inside the perforation. Experiments carried out on the heat transfer coefficient on the hot side [8,9] conclude that it is considerably different from the value assumed without injection. Ammari [10] studied the influence of coolant to mainstream density ratio and showed that for a 35 degrees injection, the heat transfer coefficient is strongly dependent on the density ratio. Nevertheless, due to the thermal conditions and the size of the perforations, there is not a detailed study of heat transfer all over a perforated plate and none can provide enough data to model heat fluxes.

2.2 Numerical studies

At the same time, RANS simulations can be performed to obtain more detailed information about the aerothermal field. But turbulence in film cooling flows is considerably anisotropic, especially around the jet exit and near to the wall [11]. Thus, the assumption of isotropic eddy-viscosity, done in the two-equation models generally used, is not adequate for film cooling calculations. In fact, using such a model produced unsatisfactory predictions of coolant film lateral spreading [12]. This is the reason why anisotropic eddy viscosity/diffusivity models have been developed [13, 14]. With simple eddy viscosity models the turbulent transport in spanwise and streamwise direction is not accounted for sufficiently, whereas in reality it should be larger to that normal to the wall [11]. To take this anisotropy into account Bergeles [14] proposed multiplying the eddy viscosity appearing in the cross Reynolds stresses by an anisotropic factor : γ (Eq. 1).

$$\mu_{t,ij} = \begin{pmatrix} \mu_t & \mu_t & \gamma\mu_t \\ \mu_t & \mu_t & \mu_t \\ \gamma\mu_t & \mu_t & \mu_t \end{pmatrix} \quad (1)$$

γ is algebraically computed as a function of the non-dimensional wall distance (Eq. 2), derived through a correlative approach based on DNS data. Numerical simulations on typical film cooling test cases and comparing the results with experimental data were performed to validate the model [15].

$$\gamma = \text{Max} \left[\frac{10^3(y^+)^{0.42}}{2.682(y^+)^2 - 5.463}, 4.25 \right] \quad (2)$$

2.3 Reference experiments

Due to the lack of results concerning heat transfer around a multi-perforated plate, a numerical database has to be created. To

compare our numerical results, the present study is based on the work of Emidio [16]. He carried out an anisothermal, full scale experiment with geometry and boundary conditions derived from modern gas turbine combustor. The influence of parameters such as blowing ratio, density ratio, pressure difference was studied. Temperature profiles along the plate are provided.

Moreover the methodology used by Mendez [2] to create his model will be followed to deduce ours. Mendez realised LES computations on the flow around a perforated plate, using a single, bi-periodic domain in order to generate a numerical database. The fluxes at the wall were post-processed in order to determine the most important contributions. The adiabatic model, designed to be used in industrial full-scale computations of gas turbine combustion chambers, is separated into a suction model and an injection model. It neglects the wall friction and reproduces the momentum fluxes at the perforated plate (injection and suction side), at a given mass flow rate and a given geometry. This model allows a good reproduction of the global structure of the flow.

2.4 Heat transfer coefficient and effectiveness

To measure thermal performance of film cooling configurations, two quantities are used, the convective heat transfer coefficient h and the adiabatic film-cooling effectiveness η_{ad} . The heat transfer coefficient is given by Eq. 3, where T_{ad} is the adiabatic wall temperature, usually presented non-dimensioned as the adiabatic film-cooling effectiveness η_{ad} (Eq. 4).

$$h = \frac{\Phi}{(T_w - T_{ad})} \quad (3)$$

$$\eta_{ad} = \frac{T_h - T_{ad}}{T_h - T_c} \quad (4)$$

T_{ad} corresponds to the temperature of an isothermal wall which is adiabatic at the local point of interest. Another parameter similar to η_{ad} also deserves mention, it is the overall effectiveness η , defined by Eq 5, which reduces the three temperature variables in the simulation to a single parameter.

$$\eta = \frac{T_h - T_w}{T_h - T_c} \quad (5)$$

In full coverage film-cooling application, a large number of geometric and aerothermal parameters influences the thermal performance. A review of these parameters is given by Bogard and Thole [17]. We only give the definition of the blowing ratio

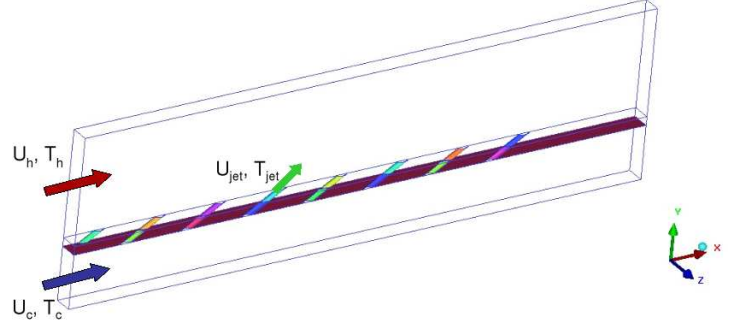


FIGURE 1. Computational domain.

(Eq. 6) which is the main aerodynamics parameter.

$$M = \frac{\rho_j U_j}{\rho_h U_h} \quad (6)$$

Indeed, this parameter is identified as the main parameter in correlation for adiabatic effectiveness by Mayle and al. [18], or as having the most important effect on the heat transfer coefficient near the hole [9].

3 NUMERICAL METHOD

3.1 Computational domain

To create a database that will enable the definition of the model, 3 dimensional conjugate heat transfer simulations are carried out with the RANS code named Cedre [19], developed at Onera. Two solvers, CHARME and ACACIA, resolve respectively RANS equations in the fluid and conduction in the solid. Each domain is solved independently using the boundary conditions produced by the other. At steady state, the temperatures as well as the heat fluxes are identical at the fluid/solid interface. The geometry used by Emidio, which consists of a plate of 18 rows of several perforations was simplified for the numerical computations : the computational domain (Fig. 1) includes a solid multi-perforated wall and two ducts, the upper one containing the hot gases (this side of the plate will be called "hot side" or "injection side"), the other containing the cold air (this side of the plate will be called "cold side" or "suction side"). The thickness of the plate is $1.6 d$, the perforations have an inclination angle of 30 degrees and are distributed in a staggered array of 15 rows. In spanwise direction, taking into account the symmetry of geometry and flow conditions, only half a perforation per row is considered. The aim of this study is not to focus on only one or two rows of perforations but to acknowledge the asymptotic evolution of heat flux and heat transfer coefficient considering the important number of rows involved in full coverage film cooling.

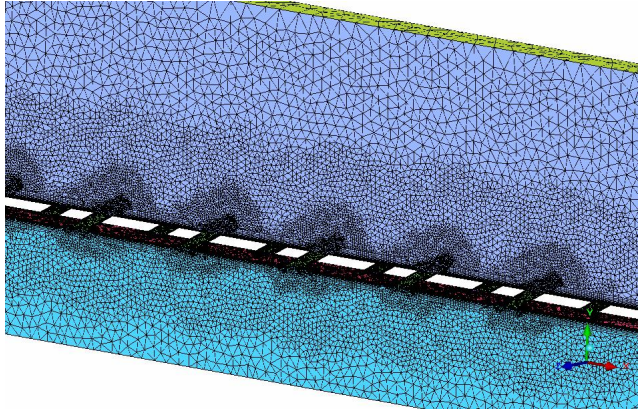


FIGURE 2. Fluid mesh.

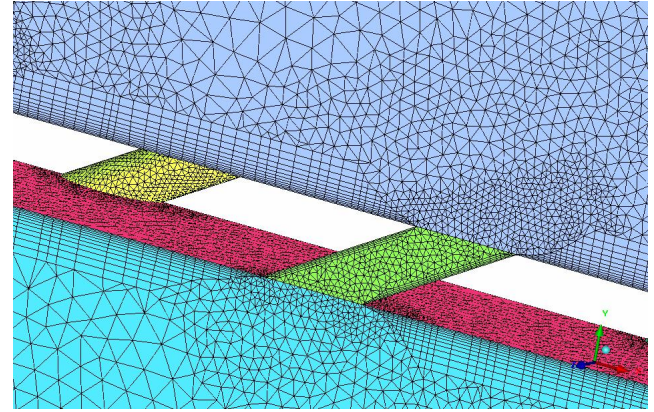


FIGURE 3. Fluid mesh detail.

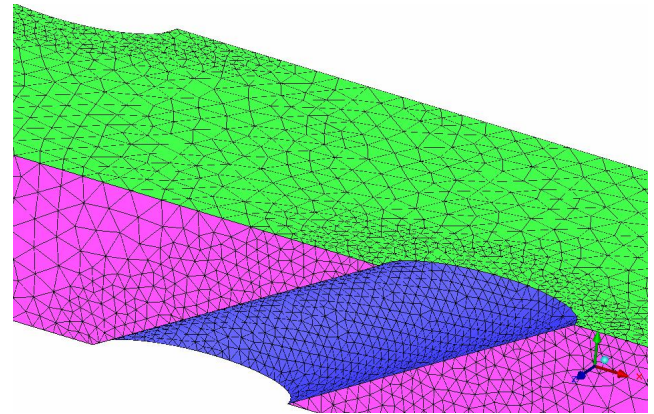


FIGURE 4. Solid mesh detail.

3.2 Computational mesh

In the fluid domain an hybrid mesh is used, with a prismatic portion close to the wall and tetrahedral mesh above (Fig. 2). In agreement with turbulence model requirements, grid was clustered near the wall so that $y^+ < 1$, when averaging on all the plate, we obtain $y_{av}^+ = 0.71$, typically first mesh point is about 5×10^{-6} millimeters above the wall. To correctly reproduce the thermal and momentum boundary layer, at least 15 cells were inserted inside the boundary layer thickness. Along the trajectory of the jets, cells density was improved. The mesh around one perforation is shown on Fig. 3. The fluid domain contains 2.5 millions nodes, 40 points describe the diameter of the hole.

The solid domain (Fig. 4) is made of one millions tetrahedral cells. Nodes at the interface between fluid and solid are coincident.

The domain was partitioned into 128 blocks. Grid independence was assessed by testing a finer mesh ($y_{av}^+ = 0.47$ and 5.1 millions nodes in the fluid domain) which resulted in a negligible change in the computed film cooling effectiveness and convective heat fluxes.

3.3 Boundary conditions

In order to reduce the size of the computational domain, the inlet is located only three hole diameters upstream the first perforation. For each simulation, the inlet boundary condition is determined from a preliminary conjugate heat transfer computation on a flat plate. Boundary conditions for this simulation were chosen to match the experimental test case as closely as possible, mass flow rate and temperature at the inlet planes and pressure at the outlet planes are the ones measured in the experiments, but no turbulence quantities are given, thus we chose to prescribe this rate to 5% in the hot channel and 1% in the cold one. A profile is extracted when the boundary layer is fully developed and the temperature of the plate is the same one as in the experiment of

Emidio. Mass flow, temperature and turbulence quantities from this profile are injected as inlet condition for both the hot and the cold duct.

A uniform pressure is applied at the outlet of each duct. Atmospheric pressure is imposed on the hot duct while the outlet pressure on the cold duct is used to impose a pressure drop that makes the cold air go through the perforation in the main duct. At both sides of the domain, symmetry boundary conditions were placed in the centreline of the effusion holes. Conjugate heat transfer condition are applied at the interface of solid and fluid domain. Temperature measured by Emidio three diameters upstream the first hole is imposed as the inlet boundary condition of the solid domain. All the other boundary conditions are adiabatic walls. The properties of the plate are the one given by the manufacturer.

3.4 Numerical simulations

Five aerothermal conditions are considered. The operating points correspond to experiments conducted by Emidio and are

Case	1	2	3	4	5
M	3.2	5.6	6.8	7.3	8.5
ΔP	4.8%	4.8%	4.8%	8.1%	5%
DR	3.75	4.44	4.6	3.81	3.8

TABLE 1. Aerothermal conditions tested.

listed in table 1.

In a first step, conjugate heat transfer simulation is performed for each case. This simulation provides heat flux, Φ , and temperature all over the plate, T_w .

Menter's SST turbulence model is used, completed with an anisotropic correction.

Calculations were performed on ONERA's Altix ICE 8200 cluster on 128 cores in order to accelerate the calculation. The global time scale is prescribed to one second, but a local time step limits the variation of all the variables to 1% at each iteration. In that case, it needs 60000 iterations to reach a converged state. Our convergence criteria is to have a variation of temperature and heat flux on the plate of less than 1% of their values in the last 10 000 iterations.

In a second step, another simulation is performed for each case replacing the conjugate heat transfer boundary condition by an adiabatic one. Thus we have access to adiabatic temperature and can deduce a local heat transfer coefficient using Eq. 3.

4 RESULTS

Results from our calculations are presented in this section. First, laterally averaged profiles of effectiveness are presented and one is compared to experimental data. To the author's view, no other data are available in the literature for such a configuration and such aerothermal conditions. Thus, only qualitative comparison will be presented concerning heat transfer coefficient. This section ends by examining the contribution of heat flux in the perforation and on the cold side to the total cooling flux and show the evolution of temperature rise through perforations.

4.1 Overall effectiveness

It is believed that turbulence model has a large influence on heat transfer. Hence in the present study a SST model with an anisotropic correction was used. It is first compared to standard SST model. Laterally averaged profiles of effectiveness along the plate obtained with the two models are confronted to the results from Emidio on Fig 5. In this figure, the origin of the x/d axis represents the centre of the first perforation. Note that due to a smaller number of rows in the computational domain, effectiveness does not reach the same top value as in the

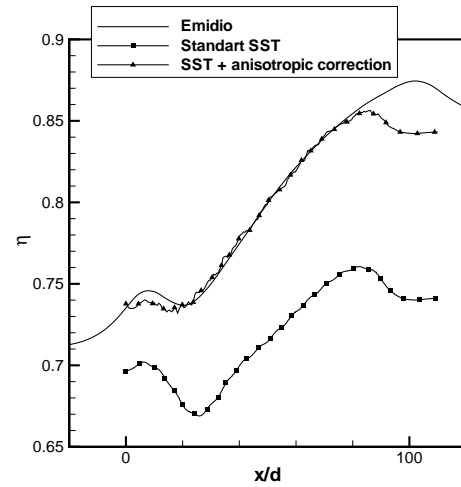


FIGURE 5. Comparison to experiment, case 3.

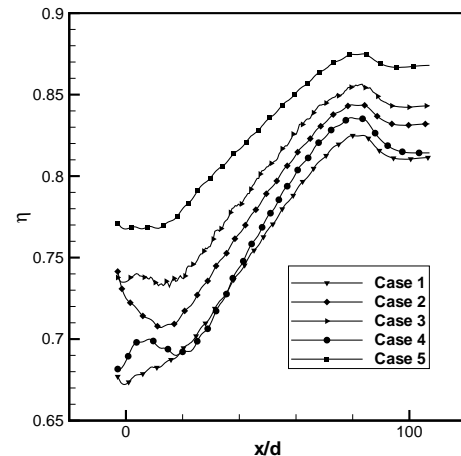


FIGURE 6. Laterally averaged profiles of overall effectiveness of the five cases.

experiments, and decrease earlier. Curve from the anisotropic calculation fit well to the experiment. Anisotropic correction provides an improvement in predicting temperature on the wall surface. All the numerical results presented in the next parts are obtained with the anisotropic correction.

The five conditions are compared in term of overall effectiveness on Fig. 6. The influence of blowing ratio can be seen, at a fixed pressure difference, effectiveness is improved when

blowing ratio increases (cases 1, 2, 3 and 5). But at a different pressure difference, the conclusion is not the same. In fact in case 4 the pressure difference is bigger thus the velocity in the perforations is stronger. The jets penetrate more in the hot flow and the interaction between them are stronger, thus more hot gases are brought close to the wall and cooling effectiveness decreases. That is why curve from case 4 is lower than expected.

4.2 Heat flux

Heat transfer coefficient has been obtained using Eq. 3. Then it has been made dimensionless with heat transfer coefficient obtained with Colburn correlation (Eq. 7).

$$Nu_0 = 0.023Re^{0.8}Pr^{0.3} \quad \text{and} \quad h_0 = \frac{Nu_0 \left(\frac{ps}{d}\right)}{\lambda} \quad (7)$$

The result of case 3 in term of coefficient ratio (h/h_0) is presented on Fig. 7(a) for the sixth hole on the cold side (the exact same structure is observed for the other perforations), this can be compared to Byerley's results on Fig. 7(b). The suction of the cold flow by the perforations increases the heat fluxes around them, suction ratio in case 3 is 1.6 that is why the enhancement is better than in Byerley example.

Thus when Colburn correlation is used to model the heat exchanged on the cold side of the multi-perforated plate, the convective heat fluxes are under estimated.

4.3 Contribution to cooling flux

A reference surface was defined as shown on Fig. 8. It can be considered around each hole on the cold side and the hot side (when holes on the left are considered, the symmetric surface will be used). Thus, to analyse the results, to each perforation will be assigned a reference surface, S_{ref} on the cold side and one on the hot side.

In the five cases, the plate is cooled on its hot side in a very small region just downstream of the hole (anywhere else on the hot side, the temperature of the fluid is hotter than the plate). This cooling flux on the hot side is negligible compared to the convective heat flux on the cold side and in the perforation. That is why we consider these two fluxes as the total cooling flux. To know the contribution of each of them, they have been respectively integrated over the hole surface and on the cold side, over the reference surface as written in Eq. 8, where $S_{exch_j} = \frac{\pi d}{2}$ is the exchange surface in half a perforation.

$$\Phi_{cooling} = \int_{S_{exch_j}} \Phi_j dS + \int_{S_{refc}} \Phi_c dS \quad (8)$$

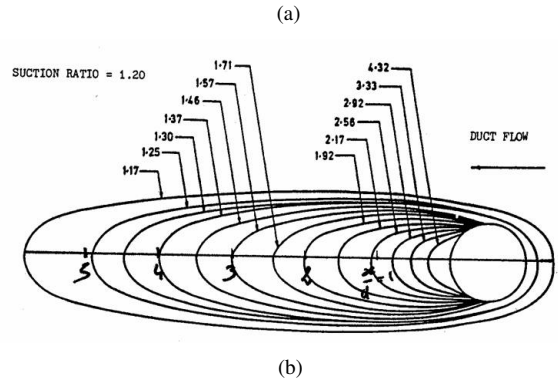
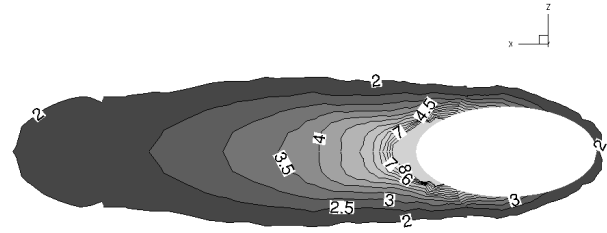


FIGURE 7. Evolution of heat transfer coefficient ratio upstream a perforation on the cold side, (a) : case 3, $Sr=1.6$, (b) : result from Byerley [5].

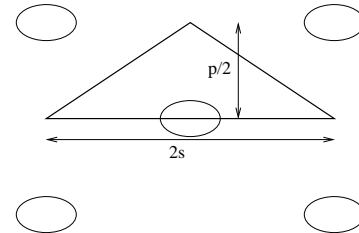


FIGURE 8. Reference surface.

Our results, presented in table 2, show that convective heat flux in the perforations can not be neglected. In fact, it represents more than 35 % of the total cooling flux, for all the rows and all the cases except the case 4, where the contribution of the perforations is more important because the pressure difference is stronger in this case.

To well reproduce the thermal behaviour of the plate, a thermal model will have to take into account the flux in each perforation.

4.4 Temperature rise in the perforations

As written above, when the solid is considered, convective heat transfer in the hole is not negligible but what are his effects on the fluid going through the perforation ?

Case	$\int_{S_{exch_j}} \Phi_j dS$	$\int_{S_{ref_c}} \Phi_c dS$
1	36 %	64 %
2	36 %	64 %
3	37 %	63 %
4	41 %	59 %
5	37 %	63 %

TABLE 2. Relative contribution of convective heat flux in a perforation and on the cold reference surface to the total cooling flux.

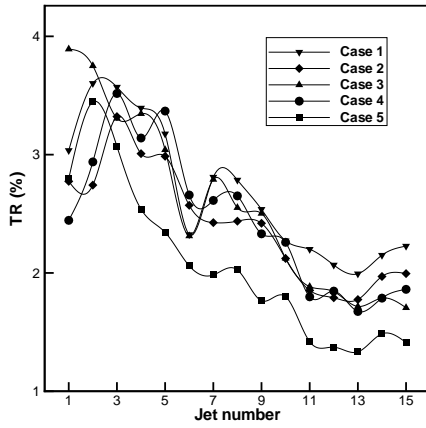


FIGURE 9. Evolution of TR in the perforations (in %).

We define the temperature rise in a perforation by the difference between the average temperature in and out of each hole. It is adimensioned as follow :

$$TR = \frac{(T_{out} - T_{in})}{(T_h - T_c)} \quad (9)$$

The evolution of the non-dimensional temperature rise in each perforation is presented in Fig. 9 for the five cases. Heating is high in the first perforations and then decreases while the plate is being cooled. Temperature rise in the perforations is not negligible and should be modelled.

Heating of the flow can be modelled, considering the heat exchanges occurring in a perforation described by Eq. 10 :

$$\rho_j C p_j U_j (T_{out} - T_{in}) \frac{\pi d^2}{4} = h_j (T_w - T_j) \pi d l \quad (10)$$

	Aspiration side	Injection side
$\int_{S_j} (\rho U_y H) dx dy$	80%	55%
$\int_{S_{solid}} (\Phi_{conv}) dx dy$	20%	45%

TABLE 3. Contribution of enthalpy flux and convective flux to the whole flux on the aspiration side and on the injection side.

4.5 Heat fluxes at the wall

On both sides of the wall, enthalpy flux and convective heat flux contribute to modify the temperature of the fluid. To know the contribution of these two fluxes, convective fluxes are integrated over the reference surface and enthalpy fluxes on the hole surface $S_j = \frac{1}{2} \left(\frac{\pi d^2}{4 \sin \alpha} \right)$ as written in Eq. 11 for the cold side and the hot side.

$$\int_{S_{ref}} (\Phi_{tot}) dx dy = \int_{S_j} (\rho U_y H) dx dy + \int_{S_{solid}} (\Phi_{conv}) dx dy \quad (11)$$

For each case, the contribution of these two fluxes to the whole flux is averaged over the 15 rows. Results are presented in table 3. On the aspiration side, enthalpy and convective fluxes are of the same importance and have to be taken into account by a thermal model to well reproduce the temperature of the flow. Whereas on the injection side, the main flux is enthalpy flux, convective heat flux is far lower and can be neglected in a first effort of modelling.

5 MODELLING THE HEAT FLUXES

Numerical simulations were performed in order to learn more about heat transfer on a multi-perforated plate. To correctly predict the wall temperature, enthalpy flux, convective heat flux on both sides of the plate and in the perforations have to be well reproduced by a thermal model. One recall that the goal of this model is not to take into account the perforation, it will not resolve the flow and the fluxes inside the plate.

To obtain homogeneous boundary condition, this part presents how enthalpy flux can be homogenised on the whole surface. In a second time, convective heat fluxes are considered, they are modelled by Eq. 12.

$$\phi = h(T_w - T_{ad}) \quad (12)$$

where h is the heat transfer coefficient. As already said in part 2.1, there are no correlation for h on the

hot side of the plate in full coverage film cooling applications. Lots of correlations exist for heat transfer coefficient in a perforation, sadly, there is no agreement between all of them. On the cold side, flat plate correlations do not take into account suction due to the presence of perforations. That is why correlations for an averaged heat transfer coefficient on each of this part have been deduced from our numerical results.

5.1 Enthalpy fluxes

Enthalpy fluxes on the inlet and the outlet of the perforation can be written as follows :

$$H_k = \int_{S_j} \rho_k C p_k U_{y_j} T_k dS \quad (13)$$

where k means either the quantities on the suction side, evaluated at T_{in} or the quantities on the ejection side evaluated at T_{out} . These fluxes should be reproduced by an homogeneous thermal model on the whole surface.

The model proposed by Mendez to homogenise the momentum fluxes will be used (this model is described in greater detail in [2]) : The whole surface can be linked to the total perforated surface by the porosity (Eq. 14) where N is the number of perforations. The normal velocity on the whole surface is deduced from the normal velocity in the perforation by Eq. 15.

$$\sigma = \frac{NS_{perf}}{S_{tot}} \quad (14)$$

$$U_{cor} = \sigma U_{y_j} \quad (15)$$

Then, the homogeneous enthalpy fluxes on the injection or the aspiration surface S_{tot} , is :

$$H_k = \int_{S_{tot}} \rho_k C p_k U_{cor} T_k dS \quad (16)$$

5.2 Heat transfer coefficient in the perforation

For a correct averaging, Eq. 12 is reformulated to give a mean value of the heat transfer coefficient in a perforation. It is obtained by averaging the heat flux, the wall temperature and the adiabatic temperature over the surface perforation.

$$\bar{h}_j = \frac{\bar{\Phi}_j}{(\bar{T}_{w_j} - \bar{T}_{ad_j})} \quad (17)$$

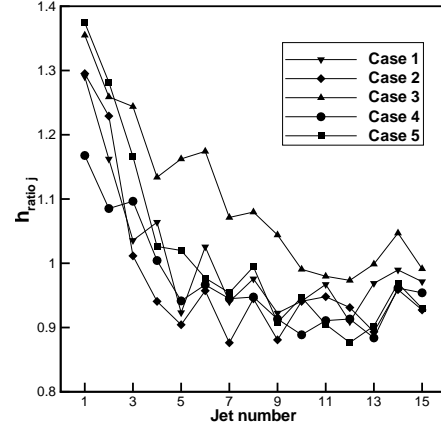


FIGURE 10. Evolution of h_{ratio_j} for the five cases.

A correlation has to be deduced from our results to well reproduce this averaged heat transfer coefficient using local data. Since no geometric parameters changes in our calculations, especially $\frac{l}{d}$, using an existing correlation for heat transfer coefficient in a perforation taking this parameter into account was necessary. Existing correlations was compared to our results. Latzko correlation (Eq. 18) is the one which gives the best result.

$$Nu_{Latzko} = 0.02775 Re_d^{0.8} \left(\frac{Re_d^{0.2}}{(\frac{l}{d})^{0.8}} \right)^{0.275} \quad (18)$$

To make this correlation better reproduce our numerical results, a correction was done to obtain : $Nu_{latzko_{cor}}$. The comparison between heat transfer coefficient obtained with this correlation and our numerical results are presented on Fig. 10 as a heat transfer coefficient ratio (Eq. 19).

$$h_{Latzko_{cor}} = \frac{Nu_{Latzko_{cor}} * \lambda_j}{d} \quad \text{and} \quad h_{ratio_j} = \frac{\bar{h}_j}{h_{Latzko_{cor}}} \quad (19)$$

The correlation does not fit the numerical results very well in the first perforations. But after four rows, the difference between the two heat transfer coefficients decreases and the ratio is close to 1 for the five cases. The deviation of the heat transfer coefficient ratio from the unity base value is relatively small to consider this correlation as a good way to obtain an average heat flux in a perforation in multi-hole film cooling applications.

5.3 Heat transfer coefficient on the cold side

An averaged heat transfer coefficient on the cold side was obtained averaging the convective heat flux, the wall temperature and the adiabatic temperature on the cold reference surface around each perforation. The averaged coefficient is calculated with Eq. 20.

$$\bar{h}_c = \frac{\bar{\phi}_c}{(\bar{T}_{w_c} - \bar{T}_{ad_c})} \quad (20)$$

Two different kinds of correlation exist concerning the cold side. Either, they were deduced from experiments where the flow on the cold side was represented by a plenum. That means no streamwise flow. These correlations depend only on the velocity in the perforation that aspirates the flow. Or, there are correlations considering a flat plate with no perforation. Suction of the flow around the hole is not taken into account.

To well reproduce the heat transfer coefficient, friction of the streamwise flow and suction, the two main phenomena, have to be taken into account. Thus two main parameters have to be used : The velocity of the streamwise flow and the velocity in the perforation.

That is why we chose to base our correlation on the Colburn correlation (Eq. 7) and the suction ratio (Eq. 21).

$$SR = \frac{V_j}{V_c} \quad (21)$$

These two parameters are used to calculate a Nusselt number as shown in Eq. 22, where C_1 and C_2 are constants fixed.

$$Nu_c = Nu_{Colburn} (1 + C_1 SR)^{C_2} \quad \text{and} \quad h_{cor_c} = \frac{Nu_c * (\frac{ps}{d})}{\lambda_c} \quad (22)$$

Results obtained are presented on Fig 11 in terms of heat transfer coefficient ratio (Eq. 23). They do not fit the numerical results in the five first perforations, but after that the ratio is close to 1.

$$h_{ratio_c} = \frac{\bar{h}_c}{h_{cor_c}} \quad (23)$$

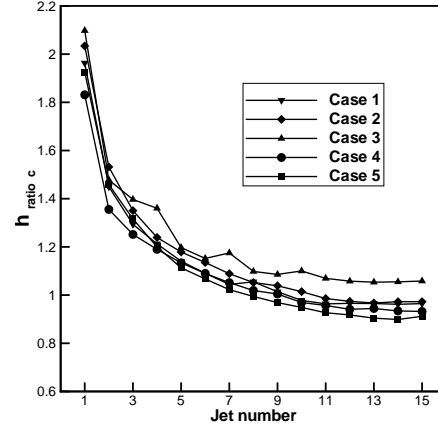


FIGURE 11. Evolution of h_{ratio_c} for the five cases.

5.4 Heat transfer coefficient on the hot side

To obtain an averaged heat transfer coefficient on the hot side, convective heat flux, wall temperature and adiabatic temperature are averaged on the hot reference surface around each perforation. The averaged coefficient is calculated with Eq. 24.

$$\bar{h}_h = \frac{\bar{\phi}_h}{(\bar{T}_{w_h} - \bar{T}_{ad_h})} \quad (24)$$

No correlation exists concerning heat transfer coefficient on the hot side of the plate. Two main parameters were isolated, the velocity ratio, $VR = \frac{V_j}{V_h}$ and the density ratio $DR = \frac{\rho_j}{\rho_h}$. A correlation for an Stanton number was defined from our results. It can be written as Eq. 25, where C_1 , C_2 and C_3 are constants fixed once and for all. This correlation has no physical meaning but is the results of curve fit procedures.

$$St_h = C_1 \cdot VR^{C_2} DR^{C_3} \quad \text{and} \quad h_{cor_h} = \rho_h C_p h U_h St_h \quad (25)$$

Results obtained with it are shown on Fig. 12 and presented as heat transfer coefficient ratio (Eq. 26) :

$$h_{ratio_h} = \frac{\bar{h}_h}{h_{cor_h}} \quad (26)$$

The correlation is able to predict a value of the heat transfer coefficient close to the numerical one except in the first perforations where heat transfer coefficient is under-estimate. This correlation can be used in a model aiming at calculating an averaged heat flux on the hot side of a multi-perforated plate.

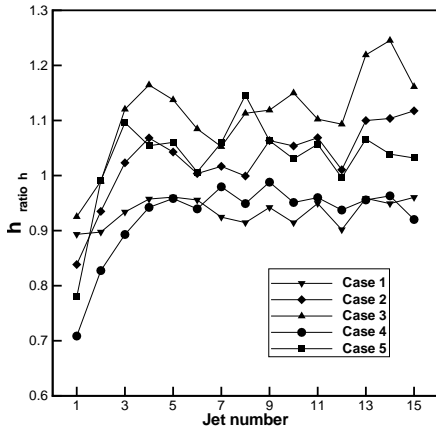


FIGURE 12. Evolution of h_{ratio_h} for the five cases.

6 CONCLUSION

In this paper, the flow over a multi-perforated plate has been simulated. Both cold side and hot side have been taken into account, the geometrical and aerothermal parameters have been chosen to reproduce an existing experiment. Numerical results fit well with experiment ones in terms of overall effectiveness. Heat transfer coefficient on both sides of the plate can not be compared to experiment data due to the lack of them in such configurations. Nevertheless, the evolution of heat transfer coefficient behind each hole on the cold side is the one expected in an experiment where only one hole is studied. Evolution of temperature rise in the perforations is presented, this heating of the flow represents around 10% of the cold temperature, thus it is not negligible and should be modelled. Convective heat fluxes in a perforation contribute to 40% to the total cooling flux and should also be modelled to well reproduce the thermal behaviour of the plate. Finally, correlations for an averaged heat transfer coefficient on the cold side, the hot side and in the perforations have been deduced.

These results will be useful in supporting future modelling efforts to account for multi-perforated plates in full scale combustion chamber calculations. Of course since only one geometry and five aerothermal conditions have been studied, correlations presented here can not be expected to be universal but as the characteristics considered in this paper are close to the practical film cooling conditions, the above conclusions can serve as a guide for further developments.

REFERENCES

[1] Lefebvre, A., 1999. "Gas turbines combustion.". *Taylor & Francis*.
 [2] Mendez, S., and Nicoud, F., 2008. "An adiabatic model for

the flow around a multi-perforated plate.". *AIAA Journal*, **46**, pp. 2623–2633.

[3] Sparrow, E., and Gurdal, U., 1981. "Heat transfer at an upstream-facing surface washed by fluid en route to an aperture in the surface.". *International Journal of Heat and Mass Transfer*, **24**(5), pp. 851–857.
 [4] Dorignac, E., Vullierme, J., Broussely, M., Foulon, C., and Mokedden, M., 2005. "Experimental heat transfer on the windward surface of a perforated flat plate.". *International Journal of Thermal Sciences*, **44**, April, pp. 885–893.
 [5] Byerley, A., Ireland, P. T., Jones, T. V., and Ashton, S., 1988. "Detailed heat transfer measurements near and within the entrance of a film cooling hole.". *ASME Paper 88-GT-155*.
 [6] Cho, H., and Goldstein, R., 1995. "Heat (mass) transfer and film effectiveness with injection through discrete holes: Part 2-on the exposed surface.". *Journal of Turbomachinery*, **117**, July, pp. 451–460.
 [7] Nguyen, P., and Dorignac, E., 2008. "Experimental study of convective exchange in a low aspect ratio perforation : Application to cooling of multiperforated wall.". *Experimental Thermal and Fluid*, **33**, July, pp. 114–122.
 [8] Eriksen, V., and Goldstein, R., 1974. "Heat transfer and film cooling following injection through inclined circular tubes.". *Journal of Heat Transfer*, May, pp. 239–245.
 [9] Kasagi, N., Hirata, M., and M.Kumada, 1981. "Studies of full coverage film cooling part 2 : Measurement of local heat transfer coefficient.". *ASME*, **81**(GT 38).
 [10] Ammari, H. D., Hay, N., and Lampard, D., 1990. "The effect of density ratio on the heat transfer coefficient from a film-cooled flat plate.". *Journal of Turbomachinery*, **112**, July, pp. 444–450.
 [11] Kaszeta, R. W., and Simon, T. W., 2000. "Measurement of eddy diffusivity of momentum in film cooling flows with streamwise injection.". *Journal of Turbomachinery*, **122**, January, pp. 178–183.
 [12] Hoda, A., and Acharya, S., 2000. "Predictions of a film coolant jet in crossflow with different turbulence models.". *Journal of Turbomachinery*, **122**, July, pp. 558–569.
 [13] Azzi, A., and Lakehal, D., 2002. "Perspectives in modeling film cooling of turbine blades by transcending conventional two-equation turbulence models.". *Journal of Turbomachinery*, **124**, July, pp. 472–484.
 [14] Bergeles, G., Gosman, A., and Launder, B., 1978. "The turbulent jet in a cross stream at low injection rates : a three-dimensional numerical treatment.". *Numerical Heat Transfer*, **1**, pp. 217–242.
 [15] Lakehal, D., 2002. "Near-wall modeling of turbulent convective heat transport in film cooling of turbine blades with the aid of direct numerical simulation data.". *Journal of Turbomachinery*, **124**, July, pp. 485–498.
 [16] Emidio, J., 1998. "Refroidissement pariétal par multi-

perforations. détermination de lois d'efficacité de refroidissement dans des conditions réelles de fonctionnement de chambres de combustion de turbines aéronautiques.”. PhD thesis, Ecole doctorale des sciences exactes et de leurs applications.

- [17] Bogard, D., and Thole, K., 2006. “Gaz turbine film cooling.”. *Journal of Propulsion and Power*, **22**(2), March-April, pp. 249–270.
- [18] Mayle, R., and Camarata, F., 1975. “Multihole cooling film effectiveness and haet transfer.”. *J. Heat Transfer*, **97**, pp. 534–538.
- [19] “<http://cedre.onera.fr>”.